
Theory-Informed Improvements to Classifier-Free Guidance for Discrete Diffusion Models

Kevin Rojas

Georgia Institute of Technology
kevin.rojas@gatech.edu

Ye He

Georgia Institute of Technology
yhe367@gatech.edu

Chieh-Hsin Lai

Sony AI
Chieh-Hsin.Lai@sony.com

Yuta Takida

Sony AI
yuta.takida@sony.com

Yuki Mitsufuji

Sony AI
yuhki.mitsufuji@sony.com

Molei Tao

Georgia Institute of Technology
mtao@gatech.edu

Abstract

Classifier-Free Guidance (CFG) is a widely used technique for conditional generation and improving sample quality in continuous diffusion models, and recent works have extended it to discrete diffusion. This paper theoretically analyzes CFG in the context of masked discrete diffusion, focusing on the role of guidance schedules. Our analysis shows that high guidance early in sampling (when inputs are heavily masked) harms generation quality, while late-stage guidance has a larger effect. These findings provide a theoretical explanation for empirical observations in recent studies on guidance schedules. The analysis also reveals an imperfection of the current CFG implementations. These implementations can unintentionally cause imbalanced transitions, such as unmasking too rapidly during the early stages of generation, which degrades the quality of the resulting samples. To address this, we draw insight from the analysis and propose a novel classifier-free guidance mechanism empirically applicable to any discrete diffusion. Intuitively, our method smoothens the transport between the data distribution and the initial (masked/uniform) distribution, which results in improved sample quality. Remarkably, our method is achievable via a simple one-line code change. The efficacy of our method is empirically demonstrated with experiments on ImageNet (masked discrete diffusion) and QM9 (uniform discrete diffusion).

1 Introduction

Continuous-state diffusion models (Ho et al., 2020; Song et al.) have proven effective in both unconditional and conditional generation tasks, such as generating data from natural language prompts. Prominent examples include text-to-image and text-to-video models like Stable Diffusion, Sora, and others (Rombach et al., 2022; Esser et al., 2024; Brooks et al., 2024). More recently, progress in discrete diffusion modeling (Campbell et al., 2022; Lou et al., 2023; Huang et al., 2023; Gruver et al., 2023; Ou et al., 2024; Shi et al., 2024; Sahoo et al., 2024) has extended the applicability of diffusion-based generation to new domains, including molecular design, protein synthesis, and languages.



Figure 1: We proposed an improved guidance mechanism through column normalization. Our method produces sharper images while being more stable to the guidance strength. Notably, it requires only a minor code modification.

Despite their success, these models often produce outputs that lack fine detail or strong alignment with conditioning inputs (e.g., text prompts). A widely adopted technique to address this issue is classifier-free guidance (CFG) (Ho and Salimans, 2021), which improves fidelity but typically at the cost of reduced sample diversity (Karras et al., 2024).

A growing body of work has sought to understand the theoretical foundations of CFG in diffusion models (Chidambaram et al., 2024; Pavasovic et al., 2025; Bradley and Nakkiran, 2024; Ye et al., 2025), while others have developed improved guidance algorithms (Karras et al., 2024; Li et al., 2024). Classifier-free guidance has also been adapted to discrete diffusion models (Nisonoff et al., 2024; Schiff et al., 2024), yielding promising empirical gains.

Among these improvements, dynamic guidance schedules—where guidance strength varies over the generation trajectory—have shown especially effective. Strategies such as guidance intervals (Kynkäänniemi et al., 2024) and gradually increasing schedules (Xi et al., 2024) can significantly enhance sample quality and are increasingly adopted in practice (Hoogeboom et al., 2024; Yu et al., 2024; Karras et al., 2024). However, such scheduling techniques remain exclusive to the continuous setting.

While recent adaptations of CFG to discrete diffusion have improved empirical performance, defining and optimizing effective guidance strategies in discrete spaces remains a fundamentally challenging and open research problem.

In our work we aim to better understand the mechanisms by which guidance affects the sampling process in discrete diffusion. Specifically, we aim to answer the following questions:

- How does the guidance schedule affect the distribution of the generated samples?
- Is it possible to characterize properties of good guidance schedules?

To do so, we start by deriving explicit formulas for the sampled distribution under varying guidance schedules in 1 and 2 dimensions. We use these expressions to study the effect of the guidance schedule. Our work leads to the following results:

- The current guidance mechanisms suffer from a flaw that complicates the simulation.
- To address the flaw, we propose a novel classifier-free guidance mechanism based on a simple yet principled column normalization of the rate matrix. This change is theoretically justified, easy to implement (pseudocode in Sec. 1), and comparing favorably to existing approaches.
- We characterize good guidance schedules for discrete diffusion.

```

def normalized_guidance_euler_transition(
    x, c, t, dt, w
):
    uncond = model(x, cond=None)
    cond = model(x, cond=c)
    logits = w * cond + (1 - w) * uncond

    p_theta = logits.softmax(dim=-1)

    s, s_bar = sigma(t), sigma_bar(t)
    change = dt * s * (1 - exp(-s_bar))
    return sample(delta(x) + change * p_theta)

```

Listing 1: Our guidance in the special case of masked diffusion using Euler transitions. Our method is a simple one line change.

```

def other_guidance_euler_transition(
    x, c, t, dt, w
):
    uncond = model(x, cond=None)
    cond = model(x, cond=c)
    logits = w * cond + (1 - w) * uncond

    p_theta = logits.exp()

    s, s_bar = sigma(t), sigma_bar(t)
    change = dt * s * (1 - exp(-s_bar))
    return sample(delta(x) + change * p_theta)

```

Listing 2: Unlocking/Simple guidance for the special case of masked diffusion using Euler transitions.

2 Preliminaries

This paper considers a vocabulary of size M and state space $S = \{1, 2, \dots, M\}^d$, with each element being a sequence of tokens. The number of tokens d will also be referred to as the dimension. Each probability distribution on S is represented as a vector in \mathbb{R}^{M^d} whose entries sum to one.

2.1 Discrete Diffusion

Given an initial distribution $p \in \mathbb{R}^{M^d}$, discrete diffusion is defined by considering a continuous time Markov chain (CTMC) given by:

$$\frac{dp_t}{dt} = R_t p_t, \quad p_0 = p. \quad (1)$$

Here $R_t \in \mathbb{R}^{M^d \times M^d}$ is known as the rate matrix, and it is such that when $t \rightarrow \infty$, p_t converges to a simple distribution. Additionally, R_t must satisfy that its non-diagonal entries are non-negative and each column must add up to zero. The time reversal of this process can be found by considering a different CTMC given by:

$$\frac{dp_{T-t}}{dt} = \bar{R}_{T-t} p_{T-t}. \quad (2)$$

This process is considered as the time reversal since it has the same law as (1) for all values of t . The reverse transition matrix can be found through the following identities:

$$\bar{R}_t(y, x) = R_t(x, y) \cdot \frac{p_t(y)}{p_t(x)}, \quad \bar{R}_t(x, x) = - \sum_{y \neq x} \bar{R}_t(y, x). \quad (3)$$

The ratios $\frac{p_t(y)}{p_t(x)}$ are called the score. Given this matrix, it is possible to generate new samples using different sampling strategies like Euler schemes, τ -leaping (Lou et al., 2023) or higher order schemes (Ren et al., 2025).

2.2 Guided Discrete Diffusion Mechanisms

There has been two approaches proposed for classifier-free guidance in discrete diffusion. We present the difference between these methods as well as that from ours in Section 3.3.

Unlocking Guidance (Nisonoff et al., 2024) introduced a guided backwards transition matrix as:

$$\bar{R}_t^{(w)}(y, x) = R_t(x, y) \cdot \left(\frac{p_t(y)}{p_t(x)} \right)^w \left(\frac{q_t(y)}{q_t(x)} \right)^{1-w}, \quad \bar{R}_t^{(w)}(x, x) = - \sum_{y \neq x} \bar{R}_t^{(w)}(y, x), \quad (4)$$

where p_t follows the forward CTMC (1) with $p_0 = p$ being the distribution that we want to conditionally generate. q_t is a sequence of guiding distribution which follows the CTMC (1) with some initial

guiding distribution $q_0 = q^1$. We will denote the **tilted distribution** by:

$$p^{(w)}(y) = Z_w^{-1} p^w(y) \cdot q^{1-w}(y), \quad Z_w = \sum_{y \in S} p^w(y) \cdot q^{1-w}(y).$$

The generation process follows the dynamics induced by the guided transition matrix:

$$\frac{dp_{T-t}}{dt} = \bar{R}_{T-t}^{(w)} p_{T-t}.$$

Applying guidance is an important step in improving the generation capabilities of diffusion models.

Simple Guidance (Schiff et al., 2024) was proposed to introduce CFG by interpolating the transition probabilities, as opposed to the rate matrix. During sampling when transitioning from time t to time $s < t$, the following transition was proposed:

$$\log p_{\text{simple}}^{(w)}(z_s | z_t) = w \log p(z_s | z_t) + (1 - w) \log q(z_s | z_t). \quad (5)$$

The transition probabilities can be obtained using the rate matrix.

2.3 Dynamic Guidance Schedules

In our work we will consider dynamic guidance schedules, i.e. making w a function of time. Such schedules have become more popular in practice. For instance, guidance interval (Hoogeboom et al., 2024; Yu et al., 2024; Karras et al., 2024) only applies guidance on a segment of the generation process. Doing so produces a boost in the performance of diffusion models. However, existing work on dynamic guidance schedules has been limited to a continuous (state-space) diffusion model. It remains unclear whether such schedules are also effective in discrete state diffusion—a question that serves as the main focus of our investigation.

Specifically, this work will consider $w : [0, T] \rightarrow \mathbb{R}$, i.e. guidance strength as a function of time, referred to as the guidance schedule. The schedule induces a generative process given by:

$$\frac{dp_{T-t}}{dt} = \bar{R}_{T-t}^{(w_{T-t})} p_{T-t} \quad (6)$$

Understanding which schedules result in the best generation is of crucial importance to further improve the sample accuracy of discrete diffusion models.

2.4 Special features of Masked Diffusion

We will focus our work on the case of masked diffusion, which is the most popular form of discrete diffusion (Ou et al., 2024; Sahoo et al., 2024; Shi et al., 2024). While our theoretical analysis is restricted to this setting, the insights it provides allow us to propose a principled improvement—specifically, a normalization strategy—that applies more broadly to the general class of discrete diffusion models, including uniform diffusion. The rate matrix in masked diffusion includes the following key structure:

$$\sigma_t \begin{pmatrix} -1 & 0 & \cdots & 0 & 0 \\ 0 & -1 & \cdots & 0 & 0 \\ \vdots & \vdots & \ddots & \vdots & \vdots \\ 0 & 0 & \cdots & -1 & 0 \\ 1 & 1 & \cdots & 1 & 0 \end{pmatrix}, \quad (7)$$

which results in a process that randomly masks each token. Once a token is masked, it remains in this state. The reverse process corresponds to progressively unmasking the tokens. During practice, the starting distribution corresponds to every token being masked.

We will use the following notations specific to masked diffusion. Let $\mathbf{x}_t = (\mathbf{x}_t^1, \dots, \mathbf{x}_t^d)$ denote a random variable on S , and M be the masked token. We will write \mathbf{x}^{UM} for the set of elements such that $\mathbf{x}_t^i \neq M$, meaning the entries that are not the masked token. Additionally, we will denote $\bar{\sigma}_t = \int_0^t \sigma_s ds$.

Masked diffusion has several appealing properties, one being the following shown by Ou et al. (2024):

¹In existing literature, p is usually a class distribution that we would like to sample from in conditional generation. q is a guiding distribution that can be chose in different ways (Karras et al., 2024; Li et al., 2024; Rojas et al., 2025). For example, in Nisonoff et al. (2024), q is the full data distribution containing different classes.

Lemma 2.1. *Along the dynamics (1) given by the masked rate matrix, if $\mathbf{x}_t = (\mathbf{x}_t^1, \dots, \mathbf{x}_t^d)$ and $\hat{\mathbf{x}}_t = (\mathbf{x}_t^1, \dots, \hat{\mathbf{x}}_t^i, \dots, \mathbf{x}_t^d)$ in such a way that $\hat{\mathbf{x}}_t^i \neq M$ and $\mathbf{x}_t^i = M$, we have the following identity for the score*

$$\frac{p_t(\hat{\mathbf{x}}_t)}{p_t(\mathbf{x}_t)} = \frac{e^{-\bar{\sigma}_t}}{1 - e^{-\bar{\sigma}_t}} p_0(\hat{\mathbf{x}}_t^i | \mathbf{x}^{UM}).$$

This result is of great importance, as it tells us that it is possible to decompose the scores as a probability distribution independent of time multiplied by a time-dependent term.

3 Methodology

Our work will be structured in the following way. In Section 3.1, we study the guided process on one token, and we demonstrate the effect of guidance in this case. We also show that in its current form, guidance suffers from a critical problem, and we introduce a method to address it in Section 3.2. Afterwards, we analyze the effect of guidance schedules on two tokens in Section 3.4. Finally, we present experimental results of our methods in Section 4.

3.1 Quantifying the exact effect of guidance in 1D Masked Diffusion

We start by studying guidance in the case where $d = 1$. In this case, the probability distribution can be represented by a simple vector. The guided rate matrix can be written as:

$$\bar{R}_t^{(w_t)} = \sigma_t \frac{e^{-\bar{\sigma}_t}}{1 - e^{-\bar{\sigma}_t}} Z_{w_t} \begin{pmatrix} 0 & \dots & 0 & p^{(w_t)}(1) \\ \vdots & \ddots & \vdots & \vdots \\ 0 & \dots & 0 & p^{(w_t)}(M-1) \\ 0 & \dots & 0 & -1 \end{pmatrix}. \quad (8)$$

This compact representation allows us to describe its dynamics in a closed-form expression:

Theorem 3.1. *Along the dynamics of equation (6), with $p_t(M) = 1$ the distribution p_0 is given by:*

$$p_0 = \frac{1}{\int_0^T \sigma_s \frac{e^{-\bar{\sigma}_s}}{1 - e^{-\bar{\sigma}_s}} Z_{w_s} ds} \cdot \int_0^T \sigma_s \frac{e^{-\bar{\sigma}_s}}{1 - e^{-\bar{\sigma}_s}} Z_{w_s} \cdot p^{(w_s)} ds. \quad (9)$$

This theorem tells us that at the terminal time, the distribution will correspond to a weighted average of tilted distributions. The total weight assigned to each distribution depends on the guidance schedule. For a version of this theorem across the whole sampling process refer to Theorem B.1.

Although this is a general result, it can be hard to assess what is the effect of the guidance schedule on the target distribution or what schedules will result in better results. To make the theoretical results more concrete, we now specialize and consider a simpler case of piecewise constant guidance.

Theorem 3.2. *Let $\delta = t_0 < t_1 < \dots < t_k = T$ be a time partition and let w_i the guidance strength on the interval $(t_i, t_{i+1}]$. Along the dynamics of equation (6), the sampled distribution p_δ is given by:*

$$p_\delta = p_T + \sum_{i=0}^{k-1} p_{t_{i+1}}(M) \cdot \left(1 - \left(\frac{1 - e^{-\bar{\sigma}_{t_i}}}{1 - e^{-\bar{\sigma}_{t_{i+1}}}} \right)^{Z_{w_i}} \right) p^{(w_i)}. \quad (10)$$

Additionally, probability mass at M at different time satisfies $p_{t_i}(M) = p_{t_{i+1}}(M) \left(\frac{1 - e^{-\bar{\sigma}_{t_i}}}{1 - e^{-\bar{\sigma}_{t_{i+1}}}} \right)^{Z_{w_i}}$ for all $i = 0, 1, \dots, k-1$.

This theorem gives a simplified interpretation of the effect of guidance schedule. Specifically, it tells us that on the interval $[t_i, t_{i+1})$ a percentage of the remaining mask will be unmasked and assigned to the tilted distribution $p^{(w_i)}$.

The key point here is that the amount of probability mass moved during the process is controlled by the weights w_i , since the partition function Z_{w_i} appears in the exponent of the rate term. This exponential dependence means even small changes in w_i can have a large effect on the transition dynamics. To demonstrate this, we consider a single segment (meaning standard constant guidance). We plot $p_t(M)$ for different values of Z_w in Figure 2. We observe that applying guidance can significantly accelerate unmasking rates. While this can lead to faster generation, it may also introduce stiffness (Rathinam et al., 2003) and inefficiencies if not properly controlled.

3.2 Improved guidance mechanisms for discrete diffusion via column normalization

In order to alleviate the *unintentional* fast unmasking rates, we propose a simple yet effective change to the guidance mechanism. To understand where this issue is coming from, note that as a consequence of Lemma 2.1, we can explicitly write the transition rates as:

$$\begin{aligned}\bar{R}_t^{(w)}(\hat{\mathbf{x}}, \mathbf{x}) &= R_t(\mathbf{x}, \hat{\mathbf{x}}) \cdot \left(\frac{p_t(\hat{\mathbf{x}})}{p_t(\mathbf{x})}\right)^w \left(\frac{q_t(\hat{\mathbf{x}})}{q_t(\mathbf{x})}\right)^{1-w} \\ &= \frac{R_t(\mathbf{x}, \hat{\mathbf{x}}) e^{-\bar{\sigma}_t}}{1 - e^{-\bar{\sigma}_t}} p_0(\hat{\mathbf{x}}^i | \mathbf{x}^{\text{UM}})^w \cdot q_0(\hat{\mathbf{x}}^i | \mathbf{x}^{\text{UM}})^{1-w}.\end{aligned}\quad (11)$$

When $w = 1$, we would end up with a probability vector on each column. However, after applying guidance, we have replaced the probability vector with an unnormalized vector, which causes the unintentional fast unmasking rates as studied in Section 3.1. Therefore, to properly apply guidance, it is necessary to normalize the columns of the guided rate matrix in equation (4) in an appropriate manner. To this end, we propose a simple but effective per-column normalization that applies to different discrete diffusion models (masked/uniform). For simplicity, we first state the per-column normalization in the case of a single token ($d = 1$).

$$\underbrace{\begin{bmatrix} \frac{p_t^w(1)q_t^{1-w}(1)}{p_t^w(x)q_t^{1-w}(x)} \\ \frac{p_t^w(2)q_t^{1-w}(2)}{p_t^w(x)q_t^{1-w}(x)} \\ \vdots \\ -\sum_{i \neq x} \frac{p_t^w(i)q_t^{1-w}(i)}{p_t^w(x)q_t^{1-w}(x)} \\ \vdots \\ \frac{p_t^w(M)q_t^{1-w}(M)}{p_t^w(x)q_t^{1-w}(x)} \end{bmatrix}}_{\text{Unnormalized vector}} \Rightarrow \underbrace{\frac{\left(\sum_{i \neq x} p_t(i)\right)^w \left(\sum_{i \neq x} q_t(i)\right)^{1-w}}{\sum_{i \neq x} p_t(i)^w q_t(i)^{1-w}}}_{\text{Normalized vector}} \cdot \begin{bmatrix} \frac{p_t^w(1)q_t^{1-w}(1)}{p_t^w(x)q_t^{1-w}(x)} \\ \frac{p_t^w(2)q_t^{1-w}(2)}{p_t^w(x)q_t^{1-w}(x)} \\ \vdots \\ -\sum_{i \neq x} \frac{p_t^w(i)q_t^{1-w}(i)}{p_t^w(x)q_t^{1-w}(x)} \\ \vdots \\ \frac{p_t^w(M)q_t^{1-w}(M)}{p_t^w(x)q_t^{1-w}(x)} \end{bmatrix}.\quad (12)$$

As seen in (12), our normalization applies to general diffusion models as long as we have access the scores for models of p, q . For the multiple-token case ($d > 1$), due to the fact that we only use one column vector that corresponds to a single-dimension jump every time, the normalization for one-token in (12) can be applied to that column vector. If we specifically consider the masked diffusion, using the parametrization in Lemma 2.1, the effective normalized rate matrix for multiple-token corresponds to simply interpolating the logits:

$$\bar{R}_{\text{nor},t}^{(w)}(\hat{\mathbf{x}}, \mathbf{x}) = \frac{R_t(\mathbf{x}, \hat{\mathbf{x}}) e^{-\bar{\sigma}_t}}{1 - e^{-\bar{\sigma}_t}} \text{Softmax}(w \log p_0(\hat{\mathbf{x}}^i | \mathbf{x}^{\text{UM}}) + (1 - w) \log q_0(\hat{\mathbf{x}}^i | \mathbf{x}^{\text{UM}})). \quad (13)$$

Interestingly, a recent extension of MaskGIT (Chang et al., 2022) known as the Halton sampler (Besnier et al., 2025) employs a form of guidance that closely resembles our approach. While MaskGIT was not originally introduced as a discrete diffusion model, it can be interpreted as such under a specific noise schedule and sampling strategy. In (Besnier et al., 2025), guidance is implemented via interpolation of the logits, which mirrors the improved implementation of classifier-free guidance mechanism that was proposed. However, this instance is a special case of our more general framework, which applies broadly to any class of discrete diffusion models. This convergence suggests that our theoretical understanding of guidance in discrete diffusion aligns with—and generalizes—the empirical strategies developed in their framework.

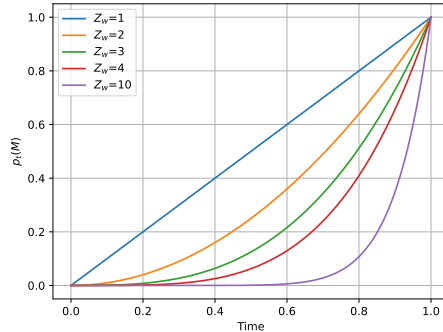


Figure 2: We plot the unmasking rates as a function of time when guidance is applied.

The normalization introduced in (12) has the effect of smoothing the transport between the starting distribution and the data distribution. We can see this theoretically in the case of masked diffusion by restating Theorem 3.2. Note that applying our guidance mechanism results in getting rid of the normalizing constant in the exponents:

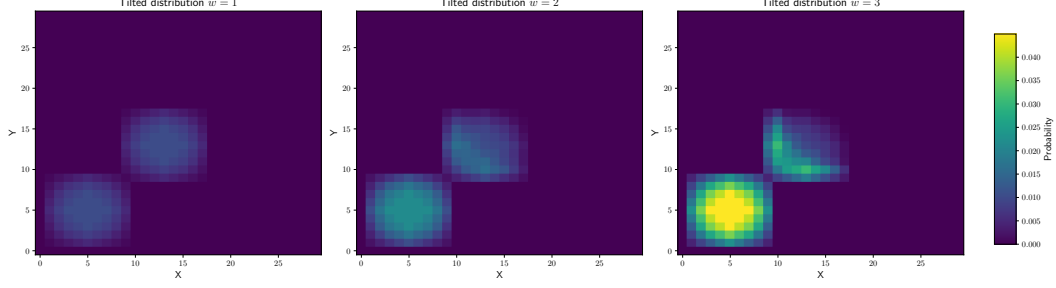


Figure 3: Tilted distributions for varying values of w . When w is large there is a larger concentration on one mode.

Theorem 3.3. Let $\delta = t_0 < t_1 < \dots < t_k = T$ be a time partition and let w_i the guidance strength on the interval $(t_i, t_{i+1}]$. Then the sampled distribution p_δ using our guidance mechanism is:

$$p_\delta = p_T + \sum_{i=0}^{k-1} p_{t_{i+1}}(M) \cdot \left(1 - \left(\frac{1 - e^{-\bar{\sigma}_{t_i}}}{1 - e^{-\bar{\sigma}_{t_{i+1}}}} \right) \right) p^{z, w_i}. \quad (14)$$

Additionally, $p_{t_i}(M) = p_{t_{i+1}}(M) \left(\frac{1 - e^{-\bar{\sigma}_{t_i}}}{1 - e^{-\bar{\sigma}_{t_{i+1}}}} \right)$.

This simple change stabilizes the sampling process and allows for a cleaner theory. We further elaborate on the experimental benefits on Section 4.

3.3 Comparison of Guidance Mechanisms

We now clarify the distinctions between the various classifier-free guidance mechanisms. While some differences between our method and that of [Nisonoff et al. \(2024\)](#) were already discussed, we further highlight how our formulation also differs from the approach of [Schiff et al. \(2024\)](#). To better understand these differences, we begin by comparing the unlocking guidance mechanism of [Nisonoff et al. \(2024\)](#) with the simple guidance proposed by [Schiff et al. \(2024\)](#). For this analysis, we keep the guidance strength fixed throughout. Notice that: $p(x_s|x_t) = \exp \left(\int_s^t \bar{R}_\tau^{(w)} d\tau \right) p_t$. Therefore, if p_t denotes the law of x_t , we can write the transition probabilities for each method:

$$p_{\text{unlocking}}(x_s|x_t) = \exp \left(\int_s^t \bar{R}_\tau^w(\cdot|c) \bar{R}_\tau^{1-w}(\cdot) d\tau \right) p_t,$$

$$p_{\text{simple}}(x_s|x_t) = Z_{\text{simple}} \left(\exp \left(\int_s^t \bar{R}_\tau(\cdot|c) d\tau \right) p_t \right)^w \left(\exp \left(\int_s^t \bar{R}_\tau(\cdot) d\tau \right) p_t \right)^{1-w}.$$

where Z_{simple} is a normalizing constant. Now we look at the w -dependence inside the exponential. For $\log p_{\text{unlocking}}$, the w -dependence is *exponential* as it appears in the exponent of the rate matrices, while for $\log p_{\text{simple}}$, the w -dependence is *linear*. Therefore, the transitions induced by the unlocking guidance method get much more aggressive when w increases. On the other hand, our normalization (depending on w) normalizes the columns so that it maintains the smoothness of the transition when w increases. Therefore our method approximates the convergence rates of the original process.

3.4 Analysis of Guidance Schedules in 2D

We now analyze the effect of guidance schedules in the case of two tokens. This case is of high interest as multiple unmaskings are done throughout the generation process. We believe that our results can be extended to higher-dimensional settings. However, the complexity of the problem grows exponentially with the number of dimensions, leading to increasingly intricate expressions and reduced interpretability. For this reason, we focus our analysis on a lower-dimensional case, where the underlying mechanisms are more transparent and the insights gained can be effectively used to improve guidance.

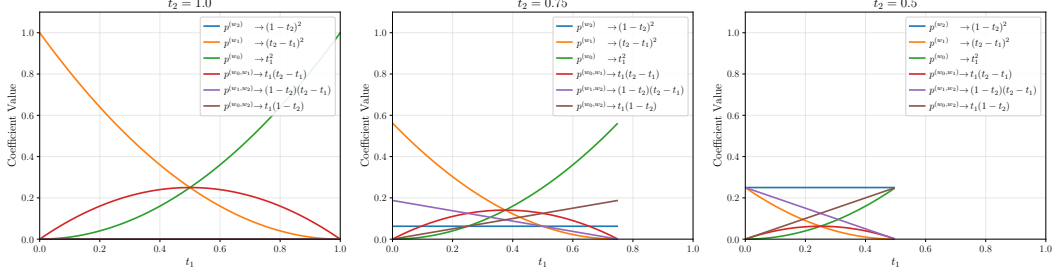


Figure 5: Evolution of the coefficients in Corollary 3.1 for different values of t_2 . Notice that we must have $t_1 \leq t_2$. We observe that for moderate t_2 no coefficient dominates others, resulting in a balanced target distribution.

To get a better intuition of the effect of guidance schedules, we perform a minor simplification using the following setup that is used in practice. We pick the log linear schedule $\bar{\sigma} = -\log(1 - \delta t)$ where δ is some small value. We then take $T = 1$ and assume that $p_T(M, M) = 1$, meaning that we initialize the distribution in a fully masked state. A consequence of our main result is the following:

Corollary 3.1. *Consider a time partition $0 = t_0 < t_1 < t_2 < t_3 = T$ with guidance w_i in the interval $[t_i, t_{i+1})$. With $\bar{\sigma} = -\log(1 - \delta t)$ and $p_T(M, M) = 1$. Then the sampled distribution follows the following formula:*

$$p_{t_0}(i, j) = \left(\frac{t_3 - t_2}{t_3}\right)^2 p^{(w_2)}(i, j) + \left(\frac{t_2 - t_1}{t_3}\right)^2 p^{(w_1)}(i, j) + \left(\frac{t_1 - t_0}{t_3}\right)^2 p^{(w_0)}(i, j) \\ + \frac{(t_3 - t_2)(t_2 - t_1)}{t_3^2} p^{(w_1, w_2)}(i, j) + \frac{(t_3 - t_2)(t_1 - t_0)}{t_3^2} p^{(w_0, w_2)}(i, j) \\ + \frac{(t_2 - t_1)(t_1 - t_0)}{t_3^2} p^{(w_0, w_1)}(i, j),$$

where $p^{(w, \gamma)}(i, j) = p^{(w)}(i, j | X_1 = i) p^{(\gamma)}(X_1 = i) + p^{(w)}(i, j | X_2 = j) p^{(\gamma)}(X_2 = j)$.

A more general version of the expression of p_t along the sampling dynamics can be found in Theorem C.1. Notice that $p^{(w, \gamma)}$ is not exactly a probability distribution as it is not necessarily normalized, but we will refer to it as one in the following discussion.

This theorem is very enlightening as it shows us two important things. First of all, it tells that guidance induces an interpolation of different distributions, which depend only on the guidance strengths. Secondly, the most significant distribution is determined by the time parameters. We analyze each of these two components separately.

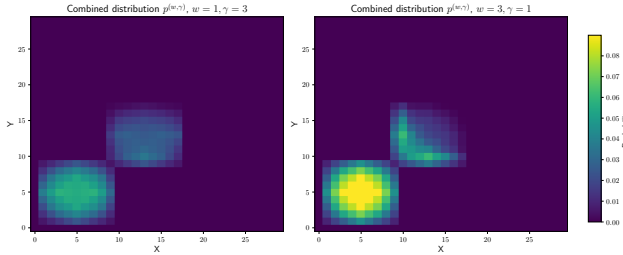


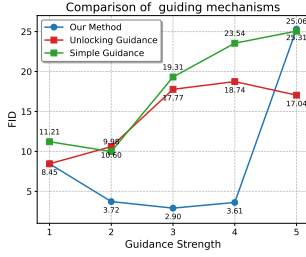
Figure 4: Combined distributions

The role of guidance weights: To understand the role of guidance weights, we consider a simple example in 2D. The data distribution has 4 clusters with 2 classes. Each class shares a section in the middle and one section in a corner. For more visualizations of the data distribution, please refer to Appendix D. We plot the tilted distribution for several values of w in Figure 3. One can observe that high values of w lead to more concentration of mass

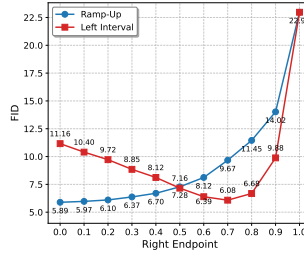
in one of the modes. We now plot $p^{(w, \gamma)}$ in Figure 4, where it can be observed that the combined distribution strongly resembles the tilted distribution of w . This means that these distributions will be more biased towards the guidance picked closer to 0; for this reason, it is preferable to have a higher guidance towards the middle and end of sampling and not at the beginning. This observation confirms the findings of Xi et al. (2024), where it was found that in practice, increasing schedules perform better.

Table 1: Comparison of several guidance schedules.

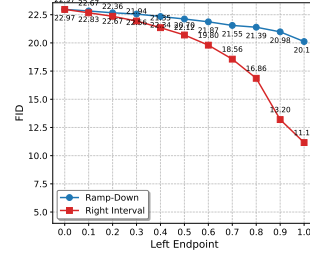
	Low G. Beg	High G. Mid	High G. End	# Params Tune	Difficulty to Tune
Constant	✗	✓	✓	1	High
Interval	✓	✓	✗	3	Low
Increasing	✓	✓	✓	1	Low
Decreasing	✗	✓	✗	1	Low



(a) Comparison of different guidance mechanisms.



(b) Right Interval vs Ramp-Up schedules.



(c) Left Interval vs Ramp-Down schedules.

Figure 6: Evaluation of different guidance mechanisms and schedules on Imagenet

The role of the time parameters: As observed in corollary 3.1, the time parameters set the proportion of each distribution that will contribute towards the final output. As observed in Figures 3,4, biasing just one of the distributions usually results in oversampling from a certain area. A good schedule is one that appropriately balances the contribution of each distribution.

We fix several values of t_2 and plot the coefficients as a function of t_1 in Figure 5. When $t_2 = 1$, we only have two intervals, and the curves change quickly; this implies that finding the right balance requires more careful tuning. On the other hand when $t_2 = .75$, many values of t_1 result in balanced combinations of all distributions, which ensures that we sample in a balanced way.

Which schedules perform best? Our theoretical analysis provides several insights into the design of effective guidance schedules. As discussed earlier, schedules that apply stronger guidance **during the middle and later stages** of the sampling process, while keeping early guidance small, tend to perform better. These selections seem to be the most critical, as they govern which distributions are mixed. Moreover, our theory predicts that using all **three intervals** (early, middle, and late) in the schedule facilitates **easier tuning** and yields more balanced output distributions. Based on these principles, we evaluate (according to our theory) various guidance schedules for discrete diffusion in Table 1, and we validate these predictions empirically in Section 4.3.

4 Numerical Results

In this section, we empirically evaluate the effectiveness of our improved guidance method (12) and explore the impact of different guidance schedules. In Section 4.1, we assess MaskGIT on the ImageNet dataset (Deng et al., 2009) at a resolution of 256×256 . Section 4.2 presents results using our guidance mechanism in the context of uniform diffusion, applied to the QM9 small molecule dataset (Ruddigkeit et al., 2012; Ramakrishnan et al., 2014). Finally, in Section 4.3, we empirically evaluate various guidance schedules in light of our theoretical findings.

4.1 Results on Imagenet

We evaluate FID on ImageNet-256 using 50K samples, following standard practices. For our method and for the Unlocking Guidance baseline (Nisonoff et al., 2024), we use the τ -leaping sampler. For Simple Guidance (Schiff et al., 2024), we interpolate Euler transitions. For all methods, we use 50 steps. Figure 6a shows FID as a function of guidance strength using a constant schedule. Our method achieves the best results by a significant margin. Furthermore, we find that failing to normalize the transition appropriately can substantially degrade sample quality.

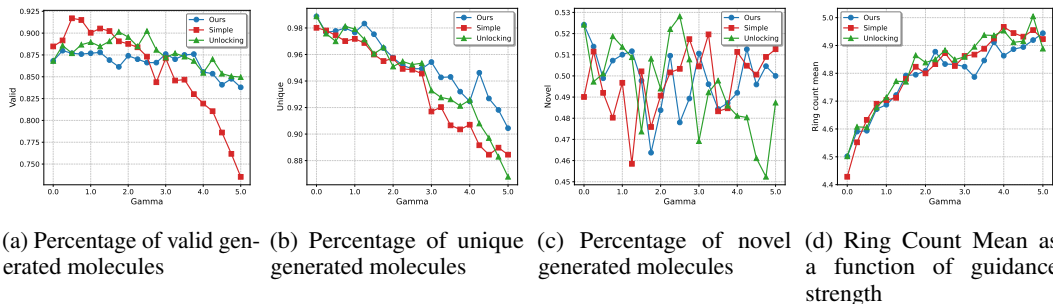


Figure 7: We display the percentage of valid, unique, and novel molecules. We find that our method is the most robust to an increase in guidance strength.

These empirical findings align with our theoretical analysis. As shown in Section 3.1, the absence of normalization leads to faster unmasking, resulting in a less smooth transport process and increased difficulty during inference. Although our method appears to deteriorate significantly at $w = 5$ in terms of quantitative metrics, the visual quality of the generated samples remains higher than those produced by other methods, we present samples in the appendix.

4.2 Results on QM9

QM9 is a dataset containing small organic molecules containing up to 9 heavy atoms. We train a conditional model on QM9 using uniform diffusion, based on the official implementation of Schiff et al. (2024), without modifying the architecture or hyperparameters. The model is conditioned on the number of rings in each molecule (ring count). Unlike ImageNet, evaluation on QM9 is more nuanced: we generate 1,024 samples and assess several metrics. First, generated molecules must satisfy chemical constraints to be considered valid. Second, a key goal of generative models is to produce novel molecules not found in the training data. Accordingly, we report both validity and novelty, along with the mean ring count (i.e., the conditioning signal), in Figure 7.

We find that our method is the most robust to increases in guidance strength. However, in general, all methods perform comparably well across the full range of strengths. This suggests that normalization may have a less pronounced effect in the uniform diffusion setting. Due to the complexity of evaluating on QM9, further experiments on additional discrete datasets are needed to more conclusively determine the optimal guidance mechanism. We leave this for future work.

4.3 Study of guidance schedules

We now perform an empirical study of guidance schedules. The schedules are summarized in Table 2. We study how these schedules perform by evaluating FID on Imagenet 256 using 10K samples. In Figure 6b we compare the Ramp-Up and Right Interval schedules. The performance of the Right Interval schedule exhibits a convex trend with respect to guidance strength, enabling straightforward tuning. In contrast, the Ramp-Up schedule shows consistently improving performance as r decreases, indicating that a gradual, linear increase in guidance outperforms abrupt alternatives. In Figure 6c we observe the performances of the Left interval and Ramp-Down schedules. It is clear that such schedules are incapable of improving the generation accuracy as suggested by our theory.

5 Conclusions

In this work, we introduced a framework for analyzing the effect of guidance schedules in masked discrete diffusion models. Our analysis leads to a novel approach for classifier-free guidance in the discrete setting. We validate the effectiveness of our method through experiments on ImageNet and show that guidance applied near $t = 0$ is particularly impactful—enabling us to identify effective

Table 2: Description of considered guidance schedules.

Schedule	Formula $w(t)$
Left Interval	$w \cdot \mathbf{1}_{[0,r]}(t)$
Right Interval	$w \cdot \mathbf{1}_{[\ell,1]}(t)$
Ramp-Up	$\min\left(w, w \cdot \frac{t}{r}\right)$
Ramp-Down	$\min\left(w, w \cdot \frac{1-t}{1-\ell}\right)$

scheduling strategies. Our theoretical insights align closely with empirical observations, bridging the gap between theory and practice.

Limitations and Future work. While our framework provides a principled and tractable approach to classifier-free guidance in discrete diffusion models, our theoretical analysis is currently limited to masked diffusion in low-dimensional settings. While the method is applicable to more complex, real-world settings, our current theoretical study does not cover such regimes. Promising directions include extending the framework to other forms of discrete diffusion, such as uniform diffusion, which warrants deeper theoretical and empirical investigation. Further questions include scaling to higher dimensions and analyzing the role of score estimation error in the guidance dynamics.

Acknowledgments and Disclosure of Funding

We thank Yuchen Zhu for helpful discussions. KR, YH, and MT are grateful for partial supports by SONY Faculty Innovation Award, NSF Grants DMS-1847802 and DMS-2513699, DOE Grant DE-NA0004261, Cullen-Peck Scholarship, and Emory-GT AI.Humanity Award.

References

- V. Besnier, M. Chen, D. Hurych, E. Valle, and M. Cord. Halton scheduler for masked generative image transformer. *arXiv preprint arXiv:2503.17076*, 2025.
- A. Bradley and P. Nakkiran. Classifier-free guidance is a predictor-corrector. *arXiv preprint arXiv:2408.09000*, 2024.
- T. Brooks, B. Peebles, C. Holmes, W. DePue, Y. Guo, L. Jing, D. Schnurr, J. Taylor, T. Luhman, E. Luhman, C. Ng, R. Wang, and A. Ramesh. Video generation models as world simulators. <https://openai.com/research/video-generation-models-as-world-simulators>, 2024.
- A. Campbell, J. Benton, V. De Bortoli, T. Rainforth, G. Deligiannidis, and A. Doucet. A continuous time framework for discrete denoising models. *Advances in Neural Information Processing Systems*, 35:28266–28279, 2022.
- H. Chang, H. Zhang, L. Jiang, C. Liu, and W. T. Freeman. Maskgit: Masked generative image transformer. In *Proceedings of the IEEE/CVF conference on computer vision and pattern recognition*, pages 11315–11325, 2022.
- M. Chidambaram, K. Gatmiry, S. Chen, H. Lee, and J. Lu. What does guidance do? a fine-grained analysis in a simple setting. In *The Thirty-eighth Annual Conference on Neural Information Processing Systems*, 2024.
- J. Deng, W. Dong, R. Socher, L.-J. Li, K. Li, and L. Fei-Fei. Imagenet: A large-scale hierarchical image database. In *2009 IEEE conference on computer vision and pattern recognition*, pages 248–255. Ieee, 2009.
- P. Esser, S. Kulal, A. Blattmann, R. Entezari, J. Müller, H. Saini, Y. Levi, D. Lorenz, A. Sauer, F. Boesel, et al. Scaling rectified flow transformers for high-resolution image synthesis. In *Forty-first international conference on machine learning*, 2024.
- N. Gruver, S. Stanton, N. Frey, T. G. Rudner, I. Hotzel, J. Lafrance-Vanasse, A. Rajpal, K. Cho, and A. G. Wilson. Protein design with guided discrete diffusion. *Advances in neural information processing systems*, 36:12489–12517, 2023.
- J. Ho and T. Salimans. Classifier-free diffusion guidance. In *NeurIPS 2021 Workshop on Deep Generative Models and Downstream Applications*, 2021.
- J. Ho, A. Jain, and P. Abbeel. Denoising diffusion probabilistic models. *Advances in neural information processing systems*, 33:6840–6851, 2020.
- E. Hoogeboom, T. Mensink, J. Heek, K. Lamerigts, R. Gao, and T. Salimans. Simpler diffusion (sid2): 1.5 fid on imagenet512 with pixel-space diffusion. *arXiv preprint arXiv:2410.19324*, 2024.
- H. Huang, L. Sun, B. Du, and W. Lv. Conditional diffusion based on discrete graph structures for molecular graph generation. In *Proceedings of the AAAI Conference on Artificial Intelligence*, volume 37, pages 4302–4311, 2023.
- T. Karras, M. Aittala, T. Kynkäänniemi, J. Lehtinen, T. Aila, and S. Laine. Guiding a diffusion model with a bad version of itself. *Advances in Neural Information Processing Systems*, 37:52996–53021, 2024.
- T. Kynkäänniemi, M. Aittala, T. Karras, S. Laine, T. Aila, and J. Lehtinen. Applying guidance in a limited interval improves sample and distribution quality in diffusion models. In *Conference on Neural Information Processing Systems*, 2024.
- T. Li, W. Luo, Z. Chen, L. Ma, and G.-J. Qi. Self-guidance: Boosting flow and diffusion generation on their own. *CoRR*, 2024.
- A. Lou, C. Meng, and S. Ermon. Discrete diffusion modeling by estimating the ratios of the data distribution. *arXiv preprint arXiv:2310.16834*, 2023.
- H. Nisonoff, J. Xiong, S. Allenspach, and J. Listgarten. Unlocking guidance for discrete state-space diffusion and flow models. *arXiv preprint arXiv:2406.01572*, 2024.

- J. Ou, S. Nie, K. Xue, F. Zhu, J. Sun, Z. Li, and C. Li. Your absorbing discrete diffusion secretly models the conditional distributions of clean data. *arXiv preprint arXiv:2406.03736*, 2024.
- K. L. Pavasovic, J. Verbeek, G. Biroli, and M. Mezard. Understanding classifier-free guidance: High-dimensional theory and non-linear generalizations. *arXiv preprint arXiv:2502.07849*, 2025.
- R. Ramakrishnan, P. O. Dral, M. Rupp, and O. A. von Lilienfeld. Quantum chemistry structures and properties of 134 kilo molecules. *Scientific Data*, 1, 2014.
- M. Rathinam, L. R. Petzold, Y. Cao, and D. T. Gillespie. Stiffness in stochastic chemically reacting systems: The implicit tau-leaping method. *The Journal of Chemical Physics*, 119(24):12784–12794, 2003.
- Y. Ren, H. Chen, Y. Zhu, W. Guo, Y. Chen, G. M. Rotskoff, M. Tao, and L. Ying. Fast solvers for discrete diffusion models: Theory and applications of high-order algorithms. *arXiv preprint arXiv:2502.00234*, 2025.
- K. Rojas, Y. Zhu, S. Zhu, F. X. Ye, and M. Tao. Diffuse everything: Multimodal diffusion models on arbitrary state spaces. In *Forty-second International Conference on Machine Learning*, 2025.
- R. Rombach, A. Blattmann, D. Lorenz, P. Esser, and B. Ommer. High-resolution image synthesis with latent diffusion models. In *Proceedings of the IEEE/CVF conference on computer vision and pattern recognition*, pages 10684–10695, 2022.
- L. Ruddigkeit, R. Van Deursen, L. C. Blum, and J.-L. Reymond. Enumeration of 166 billion organic small molecules in the chemical universe database gdb-17. *Journal of chemical information and modeling*, 52(11):2864–2875, 2012.
- S. Sahoo, M. Arriola, Y. Schiff, A. Gokaslan, E. Marroquin, J. Chiu, A. Rush, and V. Kuleshov. Simple and effective masked diffusion language models. *Advances in Neural Information Processing Systems*, 37:130136–130184, 2024.
- Y. Schiff, S. S. Sahoo, H. Phung, G. Wang, S. Boshar, H. Dalla-torre, B. P. de Almeida, A. Rush, T. Pierrot, and V. Kuleshov. Simple guidance mechanisms for discrete diffusion models. *arXiv preprint arXiv:2412.10193*, 2024.
- J. Shi, K. Han, Z. Wang, A. Doucet, and M. Titsias. Simplified and generalized masked diffusion for discrete data. *Advances in neural information processing systems*, 37:103131–103167, 2024.
- Y. Song, J. Sohl-Dickstein, D. P. Kingma, A. Kumar, S. Ermon, and B. Poole. Score-based generative modeling through stochastic differential equations. In *International Conference on Learning Representations*.
- W. Xi, N. Dufour, N. Andreou, C. Marie-Paule, V. F. Abrevaya, D. Picard, and V. Kalogeiton. Analysis of classifier-free guidance weight schedulers. *Transactions on Machine Learning Research*, 2024.
- H. Ye, R. Kevin, and T. Molei. What exactly does guidance do in masked discrete diffusion models. *arXiv preprint arXiv:2506.10971*, 2025.
- S. Yu, S. Kwak, H. Jang, J. Jeong, J. Huang, J. Shin, and S. Xie. Representation alignment for generation: Training diffusion transformers is easier than you think. *arXiv preprint arXiv:2410.06940*, 2024.

A Pseudocode for the General Setup

```
def get_normalized_rate(
    x, c, t, dt, w
):
    # Get scores
    log_score_c = get_score(x, t, cond=c)
    log_score_u = get_score(x, t, cond=None)
    log_score_w = w * log_score_c + (1-w) * log_score_u

    score_c = log_score_c.exp()
    score_u = log_score_u.exp()
    score_w = log_score_w.exp()

    # Set diagonal terms
    score_c.scatter_(-1, x[...], None, torch.zeros_like(score_c))
    score_u.scatter_(-1, x[...], None, torch.zeros_like(score_u))
    score_w.scatter_(-1, x[...], None, torch.zeros_like(score_w))

    normalized_rate = edge * score_w
    normalized_rate.scatter_(-1, x[...], None, -normalized_rate.sum(dim=-1, keepdim=True))

    # Normalize appropriately
    sum_c = score_c.sum(-1, keepdim=True) ** w
    sum_u = score_u.sum(-1, keepdim=True)
    sum_u = torch.where(sum_u > 0, sum_u**(1-w), 0)
    sum_w = score_w.sum(-1, keepdim=True)
    normalized_rate = (sum_c * sum_u / sum_w) * normalized_rate

    return sample(delta(x) + dt * sigma(t) * normalized_rate)
```

Listing 3: Our guidance in the general case using Euler transitions

B Proofs in 1D

We first prove a small lemma:

Lemma B.1. *Given a matrix of the form*

$$A = \begin{pmatrix} 0 & \dots & 0 & v_1 \\ \vdots & \vdots & \vdots & \vdots \\ 0 & \dots & 0 & v_n \end{pmatrix}$$

If $v_n \neq 0$, then its matrix exponential is given by $e^A = I + A \cdot \frac{e^{v_n} - 1}{v_n}$.

Proof. First notice that for $k > 0$ it holds that $A^k = v_n^{k-1} A$ then we can write:

$$\begin{aligned} e^A &= I + A + \frac{1}{2!}A^2 + \frac{1}{3!}A^3 + \dots \\ &= I + A + \frac{1}{2!}Av_n + \frac{1}{3!}Av_n^2 + \dots \\ &= I + A(1 + \frac{1}{2!}v_n + \frac{1}{3!}v_n^2 + \dots) \\ &= I + A(1 + \frac{1}{v_n}(\frac{1}{2!}v_n^2 + \frac{1}{3!}v_n^3 + \dots)) \\ &= I + A(1 + \frac{1}{v_n}(-1 - v_n + 1 + v_n + \frac{1}{2!}v_n^2 + \frac{1}{3!}v_n^3 + \dots)) \\ &= I + A(1 + \frac{1}{v_n}(-1 - v_n + e^{v_n})) \\ &= I + A \frac{e^{v_n} - 1}{v_n} \end{aligned}$$

As we wanted. □

We now state and prove the general version Theorem 3.1:

Theorem B.1. *Along the dynamics of equation (6). The distribution p_t is given by:*

$$p_t = \left(A_1 \cdot \frac{1 - e^A}{A}, \quad \dots, \quad A_{M-1} \cdot \frac{1 - e^A}{A}, \quad e^A \right)^\top.$$

Where, for $i = 0, \dots, M - 1$:

$$A_i = \int_t^T \sigma_s \frac{e^{-\bar{\sigma}_s}}{1 - e^{-\bar{\sigma}_s}} Z_{w_s} \cdot p^{z, w_s}(i) ds, \quad A = - \sum_{i=0}^{M-1} A_i = \int_t^T \sigma_s \frac{e^{-\bar{\sigma}_s}}{1 - e^{-\bar{\sigma}_s}} Z_{w_s} ds.$$

Proof. Recall that the rate matrix in the one-dimensional case is:

$$\bar{R}_t^{(w_t)} = \sigma_t \frac{e^{-\bar{\sigma}_t}}{1 - e^{-\bar{\sigma}_t}} Z_{w_t} \begin{pmatrix} 0 & 0 & \dots & 0 & p^{(w_t)}(1) \\ 0 & 0 & \dots & 0 & p^{(w_t)}(2) \\ \vdots & \vdots & \ddots & \vdots & \vdots \\ 0 & 0 & \dots & 0 & p^{(w_t)}(M-1) \\ 0 & 0 & \dots & 0 & -1 \end{pmatrix} \quad (15)$$

By direct integration we know that:

$$p_t = \exp \left(\int_t^T \bar{R}_\tau^{(w_\tau)} d\tau \right) p_T.$$

Therefore applying Lemma B.1 we get that (in vector notation):

$$p_t = p_T + p_T(M) \begin{pmatrix} \int_t^T \sigma_s \frac{e^{-\bar{\sigma}_s}}{1 - e^{-\bar{\sigma}_s}} Z_{w_s} \cdot p^{z, w_s} ds \cdot \frac{1 - e^A}{A} \\ e^A \end{pmatrix},$$

with

$$A = - \sum_{i=0}^{M-1} A_i = \int_t^T \sigma_s \frac{e^{-\bar{\sigma}_s}}{1 - e^{-\bar{\sigma}_s}} Z_{w_s} ds.$$

The result is proved. \square

We can now use the previous theorem to compute the distribution under constant guidance:

Corollary B.1. *If we start with a distribution p_t and keep guidance to be constant w . Then at time s the distribution is given by:*

$$p_s(i) = p_t(i) + p_s(M) \left(\frac{1 - e^{-\bar{\sigma}_t}}{1 - e^{-\bar{\sigma}_s}} - 1 \right)^{Z_w} p^{(w)}(i)$$

$$\text{for } i \neq M \text{ and } p_s(M) = \left(\frac{1 - e^{-\bar{\sigma}_t}}{1 - e^{-\bar{\sigma}_s}} - 1 \right)^{Z_w} p_t(M)$$

Proof. The proof follows by keeping w constant in the above theorem:

$$\begin{aligned} p_s &= p_t + p_t(M) \begin{pmatrix} \int_t^s \sigma_s \frac{e^{-\bar{\sigma}_s}}{1 - e^{-\bar{\sigma}_s}} Z_{w_s} \cdot p^{z, w_s} ds \cdot \frac{1 - e^A}{A} \\ e^A \end{pmatrix} \\ &= p_t + p_t(M) \begin{pmatrix} \int_t^T \sigma_s \frac{e^{-\bar{\sigma}_s}}{1 - e^{-\bar{\sigma}_s}} Z \cdot ds \cdot \frac{1 - e^A}{A} p^{(w)} \\ e^A \end{pmatrix} \\ &= p_t + p_t(M) \begin{pmatrix} (1 - e^A) p^{(w)} \\ e^A \end{pmatrix} \end{aligned}$$

Substituting A gives the desired result. \square

We can now chain the above argument to obtain a result for general piece-wise constant guidance schedules in theorem 3.2.

The results for the normalized process are identical to the ones above, so we omit them for brevity.

C Proofs in 2D

We begin by writing a simple lemma that will come in handy later.

Lemma C.1. *Given a matrix of the form*

$$A = \begin{pmatrix} 0 & a & b & 0 \\ 0 & -1 & 0 & c \\ 0 & 0 & -1 & d \\ 0 & 0 & 0 & -2 \end{pmatrix}$$

Then for any $\alpha \in \mathbb{R}$, it's matrix exponential is given by:

$$\exp(\alpha A) = \begin{pmatrix} 1 & a(1 - e^{-\alpha}) & b(1 - e^{-\alpha}) & \frac{(ac+bd)(e^\alpha-1)^2 e^{-2\alpha}}{2} \\ 0 & e^{-\alpha} & 0 & c(e^\alpha - 1)e^{-2\alpha} \\ 0 & 0 & e^{-\alpha} & d(e^\alpha - 1)e^{-2\alpha} \\ 0 & 0 & 0 & e^{-2\alpha} \end{pmatrix}$$

Proof. The proof of the above statement is easy by noticing that $A = PDP^{-1}$ with:

$$P = \begin{pmatrix} \frac{ac}{2} + \frac{bd}{2} & -a & -b & 1 \\ -c & 1 & 0 & 0 \\ -d & 0 & 1 & 0 \\ 1 & 0 & 0 & 0 \end{pmatrix}$$

$$D = \begin{pmatrix} -2 & 0 & 0 & 0 \\ 0 & -1 & 0 & 0 \\ 0 & 0 & -1 & 0 \\ 0 & 0 & 0 & 0 \end{pmatrix}$$

Then $\exp(\alpha A) = P \exp(\alpha D) P^{-1}$ and the result follows. \square

Now for the main proof we start by explicitly writing down the rate matrix in the case of two tokens. In this case the rate matrix will have the following structure:

$$\overline{R}_{\text{nor},t}^{(w)} = \frac{\sigma_t e^{-\bar{\sigma}_t}}{1 - e^{-\bar{\sigma}_t}} \begin{pmatrix} D_1 & \mathbf{0} & \dots & C_1 \\ \mathbf{0} & D_2 & \dots & C_2 \\ \vdots & \vdots & \ddots & \vdots \\ \mathbf{0} & \mathbf{0} & \mathbf{0} & L \end{pmatrix} := \frac{\sigma_t e^{-\bar{\sigma}_t}}{1 - e^{-\bar{\sigma}_t}} \overline{R}_{\text{nor}}^{(w)},$$

where each block is an $M \times M$ matrix given by the following formulas:

$$D_i = \begin{pmatrix} 0 & \dots & 0 & p^{(w)}(X_2 = 1 \mid X_1 = i) \\ 0 & \dots & 0 & p^{(w)}(X_2 = 2 \mid X_1 = i) \\ \vdots & \vdots & \vdots & \vdots \\ 0 & \dots & 0 & p^{(w)}(X_2 = M-1 \mid X_1 = i) \\ 0 & \dots & 0 & -1 \end{pmatrix}$$

$$C_i = \begin{pmatrix} p^{(w)}(X_1 = i \mid X_2 = 1) & 0 & \dots & 0 \\ \vdots & \ddots & \vdots & 0 \\ 0 & \dots & p^{(w)}(X_1 = i \mid X_2 = M-1) & 0 \\ 0 & \dots & 0 & p^{(w)}(X_1 = i) \end{pmatrix}$$

$$L = \begin{pmatrix} -1 & 0 & \dots & 0 & p^{(w)}(X_2 = 1) \\ 0 & -1 & \dots & 0 & p^{(w)}(X_2 = 2) \\ \vdots & \vdots & \ddots & \vdots & \vdots \\ 0 & \dots & 0 & -1 & p^{(w)}(X_2 = M-1) \\ 0 & \dots & 0 & 0 & -2 \end{pmatrix}$$

We can now state the main theorem:

Theorem C.1. Given a starting distribution p_t following the dynamics given by (6) the distribution at time s is given by:

$$p_s(i, j) = \begin{cases} p_t(i, j) + \left(1 - \frac{1 - e^{-\bar{\sigma}_s}}{1 - e^{-\bar{\sigma}_t}}\right)^2 p^{(w)}(i, j) p_t(M, M) \\ \quad + \left(1 - \frac{1 - e^{-\bar{\sigma}_s}}{1 - e^{-\bar{\sigma}_t}}\right) \left[p^{(w)}(X_2 = j \mid X_1 = i) p_t(i, M) \right. \\ \quad \left. + p^{(w)}(X_1 = i \mid X_2 = j) p_t(M, j) \right] & \text{if } i, j \neq M \\ \left(\frac{1 - e^{-\bar{\sigma}_s}}{1 - e^{-\bar{\sigma}_t}} \right) p_t(i, M) \\ \quad + \left(\frac{1 - e^{-\bar{\sigma}_s}}{1 - e^{-\bar{\sigma}_t}} \right)^2 \left(\frac{1 - e^{-\bar{\sigma}_t}}{1 - e^{-\bar{\sigma}_s}} - 1 \right) p^{(w)}(X_1 = i) p_t(M, M) & \text{if } i \neq M, j = M \\ \left(\frac{1 - e^{-\bar{\sigma}_s}}{1 - e^{-\bar{\sigma}_t}} \right) p_t(M, j) \\ \quad + \left(\frac{1 - e^{-\bar{\sigma}_s}}{1 - e^{-\bar{\sigma}_t}} \right)^2 \left(\frac{1 - e^{-\bar{\sigma}_t}}{1 - e^{-\bar{\sigma}_s}} - 1 \right) p^{(w)}(X_2 = j) p_t(M, M) & \text{if } i = M, j \neq M \\ \left(\frac{1 - e^{-\bar{\sigma}_s}}{1 - e^{-\bar{\sigma}_t}} \right)^2 p_t(M, M) & \text{if } i = j = M \end{cases}$$

Proof. By direct integration we know that:

$$p_s = \exp \left(\int_s^t \frac{\sigma_\tau e^{-\bar{\sigma}_\tau}}{1 - e^{-\bar{\sigma}_\tau}} d\tau \bar{R}_{\text{nor}}^{(w)} \right) = \exp \left(\ln \left(\frac{1 - e^{-\bar{\sigma}_t}}{1 - e^{-\bar{\sigma}_s}} \right) \bar{R}_{\text{nor}}^{(w)} \right).$$

Due to the block structure of $\bar{R}_{\text{nor}}^{(w)}$, it is enough to be able to compute the exponential of:

$$\begin{pmatrix} D_i & C_i \\ \mathbf{0} & L \end{pmatrix} = \left[\begin{array}{cccc|cccc} 0 & \dots & 0 & p^{(w)}(X_2 = 1 \mid X_1 = i) & p^{(w)}(X_1 = i \mid X_2 = 1) & 0 & \dots & 0 \\ 0 & \dots & 0 & p^{(w)}(X_2 = 2 \mid X_1 = i) & \vdots & \ddots & \vdots & 0 \\ \vdots & \vdots & \vdots & \vdots & 0 & \dots & 0 & 0 \\ 0 & \dots & 0 & -1 & 0 & \dots & 0 & p^{(w)}(X_1 = i) \\ \hline 0 & \dots & 0 & 0 & -1 & 0 & \dots & p^{(w)}(X_2 = 1) \\ 0 & \dots & 0 & 0 & 0 & -1 & \dots & p^{(w)}(X_2 = 2) \\ \vdots & \vdots & \vdots & \vdots & \vdots & \vdots & \ddots & \vdots \\ 0 & \dots & 0 & 0 & 0 & \dots & 0 & -2 \end{array} \right]$$

where once again we can exploit the structured form of the matrix to simplify the calculation. It is clear that when computing products of this matrix, coordinates will only get affected by the smaller subblocks:

$$\left(\begin{array}{cc|cc} 0 & p^{(w)}(X_2 = j \mid X_1 = i) & p^{(w)}(X_1 = i \mid X_2 = j) & 0 \\ 0 & -1 & 0 & p^{(w)}(X_1 = i) \\ \hline 0 & 0 & -1 & p^{(w)}(X_2 = j) \\ 0 & 0 & 0 & -2 \end{array} \right)$$

This is not only clear from the structure, but it also reveals a true intuitive understanding. The probability mass at a given position can only be affected by those states that are reachable from the current state by masking or unmasking the entries. We can now use Lemma C.1 to find the

exponential:

$$\begin{pmatrix} 1 & p^{(w)}(X_2 = j \mid X_1 = i)(1 - e^{-\alpha}) & p^{(w)}(X_1 = i \mid X_2 = j)(1 - e^{-\alpha}) & p^{(w)}(i, j)(e^\alpha - 1)^2 e^{-2\alpha} \\ 0 & e^{-\alpha} & 0 & p^{(w)}(X_1 = i)(e^\alpha - 1) e^{-2\alpha} \\ 0 & 0 & e^{-\alpha} & p^{(w)}(X_2 = j)(e^\alpha - 1) e^{-2\alpha} \\ 0 & 0 & 0 & e^{-2\alpha} \end{pmatrix}$$

where $\alpha = \ln \left(\frac{1 - e^{-\bar{\sigma}_t}}{1 - e^{-\bar{\sigma}_s}} \right)$ and we used that $2p^{(w)}(i, j) = p^{(w)}(X_2 = j \mid X_1 = i)p^{(w)}(X_1 = i) + p^{(w)}(X_1 = i \mid X_2 = j)p^{(w)}(X_2 = j)$. Putting this together, we get that exponentiation each block we get:

$$\left[\begin{array}{ccc|ccc} 1 & \dots & 0 & p^{(w)}(X_2 = 1 \mid X_1 = i)(1 - e^{-\alpha}) & p^{(w)}(X_1 = i \mid X_2 = 1)(1 - e^{-\alpha}) & \dots & p^{(w)}(i, 1)(e^\alpha - 1)^2 e^{-2\alpha} \\ 0 & \dots & 0 & p^{(w)}(X_2 = 2 \mid X_1 = i)(1 - e^{-\alpha}) & \vdots & \ddots & p^{(w)}(i, 1)(e^\alpha - 1)^2 e^{-2\alpha} \\ \vdots & \vdots & \vdots & \vdots & 0 & & \vdots \\ 0 & \dots & 0 & e^{-\alpha} & 0 & \dots & p^{(w)}(X_1 = i)(1 - e^\alpha) e^{-2\alpha} \\ \hline 0 & \dots & 0 & 0 & e^{-\alpha} & \dots & p^{(w)}(X_2 = 1)(1 - e^\alpha) e^{-2\alpha} \\ 0 & \dots & 0 & 0 & 0 & e^{-\alpha} \dots & p^{(w)}(X_2 = 2)(1 - e^\alpha) e^{-2\alpha} \\ \vdots & \vdots & \vdots & \vdots & \vdots & \ddots & \vdots \\ 0 & \dots & 0 & 0 & 0 & \dots & e^{-2\alpha} \end{array} \right]$$

With this, we have a full characterization of the matrix exponential. Therefore, we can simply write down the probability distribution by multiplying by p_t :

$$p_s(i, j) = \begin{cases} p_t(i, j) + (1 - e^{-\alpha})^2 p^{(w)}(i, j) p_t(M, M) \\ \quad + (1 - e^{-\alpha}) \left[p^{(w)}(X_2 = j \mid X_1 = i) p_t(i, M) \right. \\ \quad \left. + p^{(w)}(X_1 = i \mid X_2 = j) p_t(M, j) \right] & \text{if } i, j \neq M \\ e^{-\alpha} p_t(i, M) \\ \quad + e^{-2\alpha} (e^\alpha - 1) p^{(w)}(X_1 = i) p_t(M, M) & \text{if } i \neq M, j = M \\ e^{-\alpha} p_t(M, j) \\ \quad + e^{-2\alpha} (e^\alpha - 1) p^{(w)}(X_2 = j) p_t(M, M) & \text{if } i = M, j \neq M \\ e^{-2\alpha} p_t(M, M) & \text{if } i = j = M \end{cases}$$

We can now replace $\alpha = \ln \left(\frac{1 - e^{-\bar{\sigma}_t}}{1 - e^{-\bar{\sigma}_s}} \right)$ into the formula above to obtain the result.

□

Corollary C.1. Given a starting distribution p_t following the dynamics given by (6) with $\bar{\sigma}_t = -\log(1 - \delta t)$ the distribution at time s is given by:

$$p_s(i, j) = \begin{cases} p_t(i, j) + \left(\frac{t-s}{t}\right)^2 p^{(w)}(i, j) p_t(M, M) \\ \quad + \left(\frac{t-s}{t}\right) \left[p^{(w)}(X_2 = j | X_1 = i) p_t(i, M) \right. \\ \quad \left. + p^{(w)}(X_1 = i | X_2 = j) p_t(M, j) \right] & \text{if } i, j \neq M \\ \frac{s}{t} \cdot p_t(i, M) + \left(\frac{s}{t}\right)^2 \left(\frac{t-s}{s}\right) p^{(w)}(X_1 = i) p_t(M, M) & \text{if } i \neq M, j = M \\ \frac{s}{t} \cdot p_t(M, j) + \left(\frac{s}{t}\right)^2 \left(\frac{t-s}{s}\right) p^{(w)}(X_2 = j) p_t(M, M) & \text{if } i = M, j \neq M \\ \left(\frac{s}{t}\right)^2 p_t(M, M) & \text{if } i = j = M \end{cases}$$

Proof. Notice that under this schedule we have that:

$$\frac{1 - e^{-\bar{\sigma}_s}}{1 - e^{-\bar{\sigma}_t}} = \frac{\delta s}{\delta t} = \frac{s}{t}$$

Substituting this in gives the corollary above. \square

Proof of Corollary 3.1. We track the changes in the distribution in every time interval. This can be found by plugging in the result of the corollary above. Firstly, on the interval $T \rightarrow t_2$ we obtain:

$$\begin{aligned} p_{t_2}(M, M) &= \left(\frac{t_2}{T}\right)^2 \\ p_{t_2}(M, j) &= \left(\frac{t_2}{T}\right)^2 \left(\frac{T-t_2}{t_2}\right) p^{(w_2)}(X_2 = j) \\ p_{t_2}(i, M) &= \left(\frac{t_2}{T}\right)^2 \left(\frac{T-t_2}{t_2}\right) p^{(w_2)}(X_1 = i) \\ p_{t_2}(i, j) &= \left(\frac{T-t_2}{T}\right)^2 p^{(w_2)}(i, j) \end{aligned}$$

Then on the interval from $t_2 \rightarrow t_1$ we get:

$$\begin{aligned} p_{t_1}(M, M) &= \left(\frac{t_1}{T}\right)^2 \\ p_{t_1}(M, j) &= \left(\frac{t_1}{t_2}\right) p_{t_2}(M, j) + \left(\frac{t_1}{t_2}\right)^2 \left(\frac{t_2-t_1}{t_1}\right) p^{(w_1)}(X_2 = j) p_{t_2}(M, M) \\ p_{t_1}(i, M) &= \left(\frac{t_1}{t_2}\right) p_{t_2}(i, M) + \left(\frac{t_1}{t_2}\right)^2 \left(\frac{t_2-t_1}{t_1}\right) p^{(w_1)}(X_1 = i) p_{t_2}(M, M) \\ p_{t_1}(i, j) &= p_{t_2}(i, j) + \left(\frac{t_2-t_1}{t_2}\right)^2 p^{(w_1)}(i, j) p_{t_2}(M, M) \\ &\quad + \left(\frac{t_2-t_1}{t_2}\right) [p^{(w_1)}(X_2 = j | X_1 = i) p_{t_2}(i, M) + p^{(w_1)}(X_1 = i | X_2 = j) p_{t_2}(M, j)] \end{aligned}$$

Replacing the values for p_{t_1} into this equation we get:

$$p_{t_1}(M, M) = \left(\frac{t_1}{T}\right)^2$$

$$\begin{aligned}
p_{t_1}(M, j) &= \left(\frac{t_1(T-t_2)}{T^2} \right) p^{(w_2)}(X_2 = j) + \left(\frac{t_1}{T} \right)^2 \left(\frac{t_2-t_1}{t_1} \right) p^{(w_2)}(X_2 = j) \\
p_{t_1}(i, M) &= \left(\frac{t_1(T-t_2)}{T^2} \right) p^{(w_2)}(X_1 = i) + \left(\frac{t_1}{T} \right)^2 \left(\frac{t_2-t_1}{t_1} \right) p^{(w_2)}(X_1 = i) \\
p_{t_1}(i, j) &= \left(\frac{T-t_2}{T} \right)^2 p^{(w_2)}(i, j) + \left(\frac{t_2-t_1}{t_2} \right)^2 \left(\frac{t_2}{T} \right)^2 p^{(w_1)}(i, j) \\
&\quad + \left(\frac{t_2-t_1}{t_2} \right) \left(\frac{t_2}{T} \right)^2 \left(\frac{T-t_2}{t_2} \right) p^{(w_1)}(X_2 = j | X_1 = i) p^{(w_2)}(X_1 = i) \\
&\quad + \left(\frac{t_2-t_1}{t_2} \right) \left(\frac{t_2}{T} \right)^2 \left(\frac{T-t_2}{t_2} \right) p^{(w_1)}(X_1 = i | X_2 = j) p^{(w_2)}(X_2 = j) \\
&= \left(\frac{T-t_2}{T} \right)^2 p^{(w_2)}(i, j) + \left(\frac{t_2-t_1}{T} \right)^2 p^{(w_1)}(i, j) + \frac{(t_2-t_1)(T-t_2)}{T^2} p^{(w_1, w_2)}
\end{aligned}$$

Finally, we can proceed with the final step from $t_1 \rightarrow t_0$. In this case, we have:

$$\begin{aligned}
p_{t_0}(M, M) &= 0 \\
p_{t_0}(M, j) &= 0 \\
p_{t_0}(i, M) &= 0 \\
p_{t_0}(i, j) &= p_{t_1}(i, j) + \left(\frac{t_1-t_0}{t_1} \right)^2 p^{(w_0)}(i, j) p_{t_1}(M, M) \\
&\quad + \left(\frac{t_1-t_0}{t_1} \right) [p^{(w_0)}(X_2 = j | X_1 = i) p_{t_1}(i, M) + p^{(w_0)}(X_1 = i | X_2 = j) p_{t_1}(M, j)]
\end{aligned}$$

Then substituting in the previous results:

$$\begin{aligned}
p_{t_0}(i, j) &= p_{t_1}(i, j) + \left(\frac{t_1-t_0}{t_1} \right)^2 \left(\frac{t_1}{T} \right)^2 p^{(w_0)}(i, j) \\
&\quad + \left(\frac{t_1-t_0}{t_1} \right) \left[p^{(w_0)}(X_2 = j | X_1 = i) \right. \\
&\quad \left. \left(\frac{t_1(T-t_2)}{T^2} p^{(w_2)}(X_1 = i) + \left(\frac{t_1}{T} \right)^2 \left(\frac{t_2-t_1}{t_1} \right) p^{(w_2)}(X_1 = i) \right) \right. \\
&\quad \left. + p^{(w_0)}(X_1 = i | X_2 = j) \right. \\
&\quad \left. \left(\frac{t_1(T-t_2)}{T^2} p^{(w_2)}(X_2 = j) + \left(\frac{t_1}{T} \right)^2 \left(\frac{t_2-t_1}{t_1} \right) p^{(w_2)}(X_2 = j) \right) \right]
\end{aligned}$$

Grouping by coefficient we get:

$$\begin{aligned}
p_{t_0}(i, j) &= p_{t_1}(i, j) + \left(\frac{t_1-t_0}{t_1} \right)^2 \left(\frac{t_1}{T} \right)^2 p^{(w_0)}(i, j) \\
&\quad + \left(\frac{t_1-t_0}{t_1} \right) \cdot \\
&\quad \left[\left(\frac{t_1(T-t_2)}{T^2} \right) [p^{(w_0)}(X_2 = j | X_1 = i) p^{(w_2)}(X_1 = i) + p^{(w_0)}(X_1 = i | X_2 = j) p^{(w_2)}(X_2 = j)] \right. \\
&\quad \left. + \left(\frac{t_1}{T} \right)^2 \left(\frac{t_2-t_1}{t_1} \right) [p^{(w_0)}(X_2 = j | X_1 = i) p^{(w_1)}(X_1 = i) + p^{(w_0)}(X_1 = i | X_2 = j) p^{(w_1)}(X_2 = j)] \right] \\
&= p_{t_1}(i, j) + \left(\frac{t_1-t_0}{t_1} \right)^2 \left(\frac{t_1}{T} \right)^2 p^{(w_0)}(i, j)
\end{aligned}$$

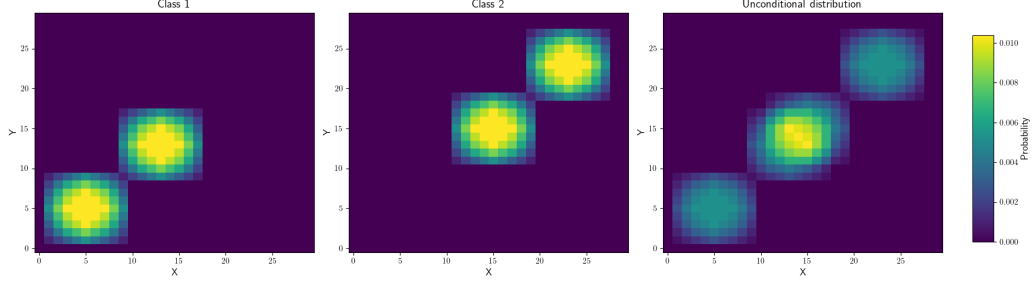


Figure 8: Definitions of the class and unconditional distributions for the toy problem.

$$+ \left(\frac{t_1 - t_0}{t_1} \right) \cdot \left[\frac{t_1(T - t_2)}{T^2} p^{(w_0, w_2)} + \left(\frac{t_1}{T} \right)^2 \left(\frac{t_2 - t_1}{t_1} \right) p^{(w_0, w_1)} \right]$$

Simplifying and substituting the term of p_{t_1} this becomes:

$$\begin{aligned} p_{t_0}(i, j) &= \left(\frac{t_3 - t_2}{t_3} \right)^2 p^{(w_2)}(i, j) + \left(\frac{t_2 - t_1}{t_3} \right)^2 p^{(w_1)}(i, j) + \left(\frac{t_1 - t_0}{t_3} \right)^2 p^{(w_0)}(i, j) \\ &+ \frac{(t_3 - t_2)(t_2 - t_1)}{t_3^2} p^{(w_1, w_2)}(i, j) + \frac{(t_3 - t_2)(t_1 - t_0)}{t_3^2} p^{(w_0, w_2)}(i, j) \\ &+ \frac{(t_2 - t_1)(t_1 - t_0)}{t_3^2} p^{(w_0, w_1)}(i, j). \end{aligned}$$

□

D Details on toy example

We now present the details of the toy example that we used to demonstrate our theoretical results. In figure 8 we present plots of each class and the full data distribution. Each cluster is defined via the following matrix

$$\begin{bmatrix} 0.1 & 0.2 & 0.3 & 0.4 & 0.5 & 0.4 & 0.3 & 0.2 & 0.1 \\ 0.2 & 0.4 & 0.6 & 0.7 & 0.8 & 0.7 & 0.6 & 0.4 & 0.2 \\ 0.3 & 0.6 & 0.8 & 0.9 & 1.0 & 0.9 & 0.8 & 0.6 & 0.3 \\ 0.4 & 0.7 & 0.9 & 1.0 & 1.0 & 1.0 & 0.9 & 0.7 & 0.4 \\ 0.5 & 0.8 & 1.0 & 1.0 & 1.0 & 1.0 & 1.0 & 0.8 & 0.5 \\ 0.4 & 0.7 & 0.9 & 1.0 & 1.0 & 1.0 & 0.9 & 0.7 & 0.4 \\ 0.3 & 0.6 & 0.8 & 0.9 & 1.0 & 0.9 & 0.8 & 0.6 & 0.3 \\ 0.2 & 0.4 & 0.6 & 0.7 & 0.8 & 0.7 & 0.6 & 0.4 & 0.2 \\ 0.1 & 0.2 & 0.3 & 0.4 & 0.5 & 0.4 & 0.3 & 0.2 & 0.1 \end{bmatrix}$$

Each class is equally weighted. A pseudocode for generating the above dataset is:

```
height, width = 30, 30

matrix1 = torch.zeros((height, width))
matrix1[1:10, 1:10] = torch.tensor(cluster)
matrix1[9:18, 9:18] = torch.tensor(cluster)

matrix2 = torch.zeros((height, width))
matrix2[11:20, 11:20] = torch.tensor(cluster)
matrix2[19:28, 19:28] = torch.tensor(cluster)
```

Listing 4: Code to generate our toy dataset

E Generated samples from our method

To generate these samples we made use of a single node with 8 NVIDIA A100 GPUs. We present samples to compare our method against other guidance methods.

E.1 Guidance strength $w = 2$



Figure 9: Comparison of samples generated by different guidance methods across various seeds or configurations.

E.2 Guidance strength $w = 3$

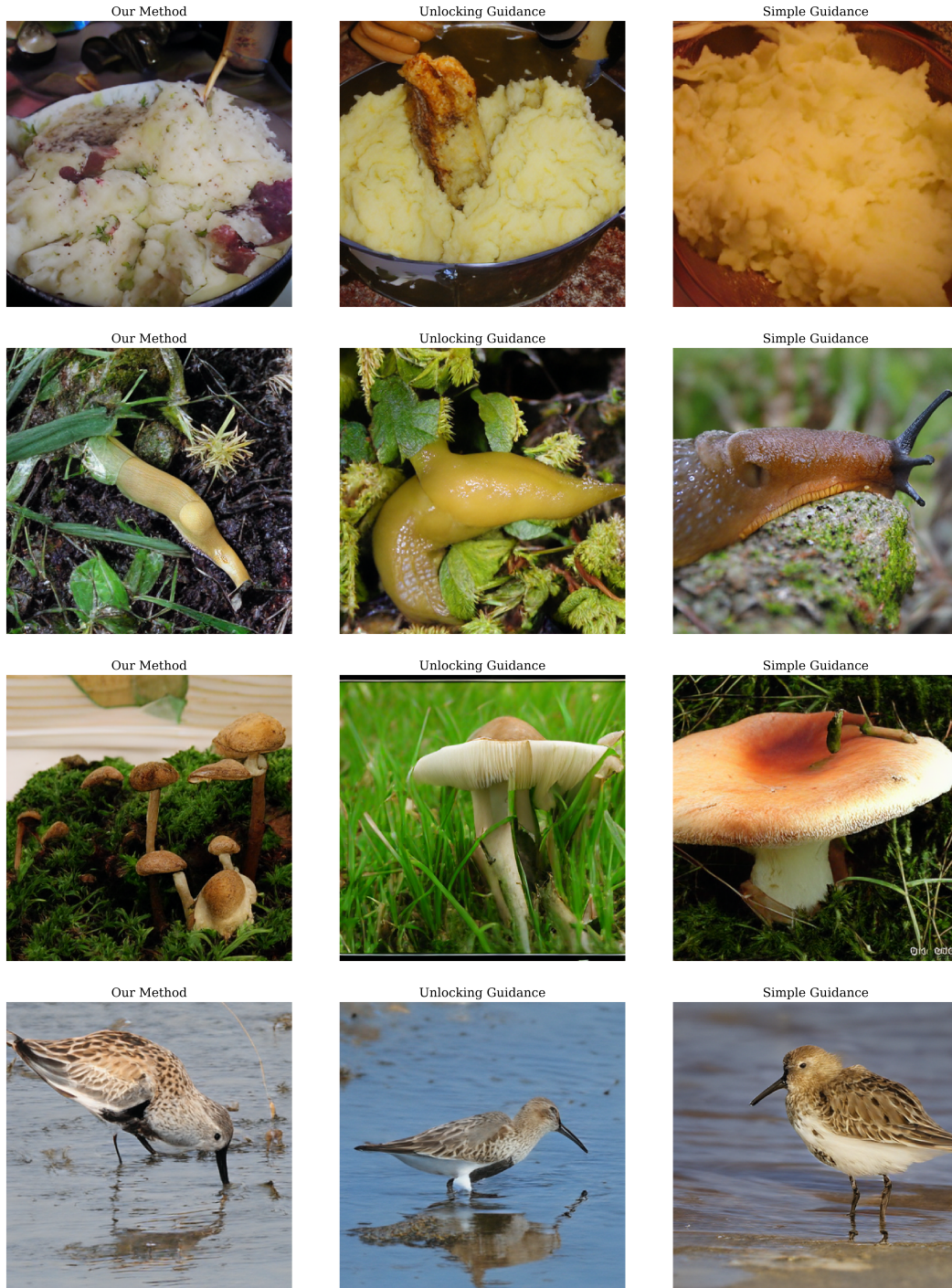


Figure 10: Comparison of samples generated by different guidance methods across various seeds or configurations.

E.3 Guidance strength $w = 4$

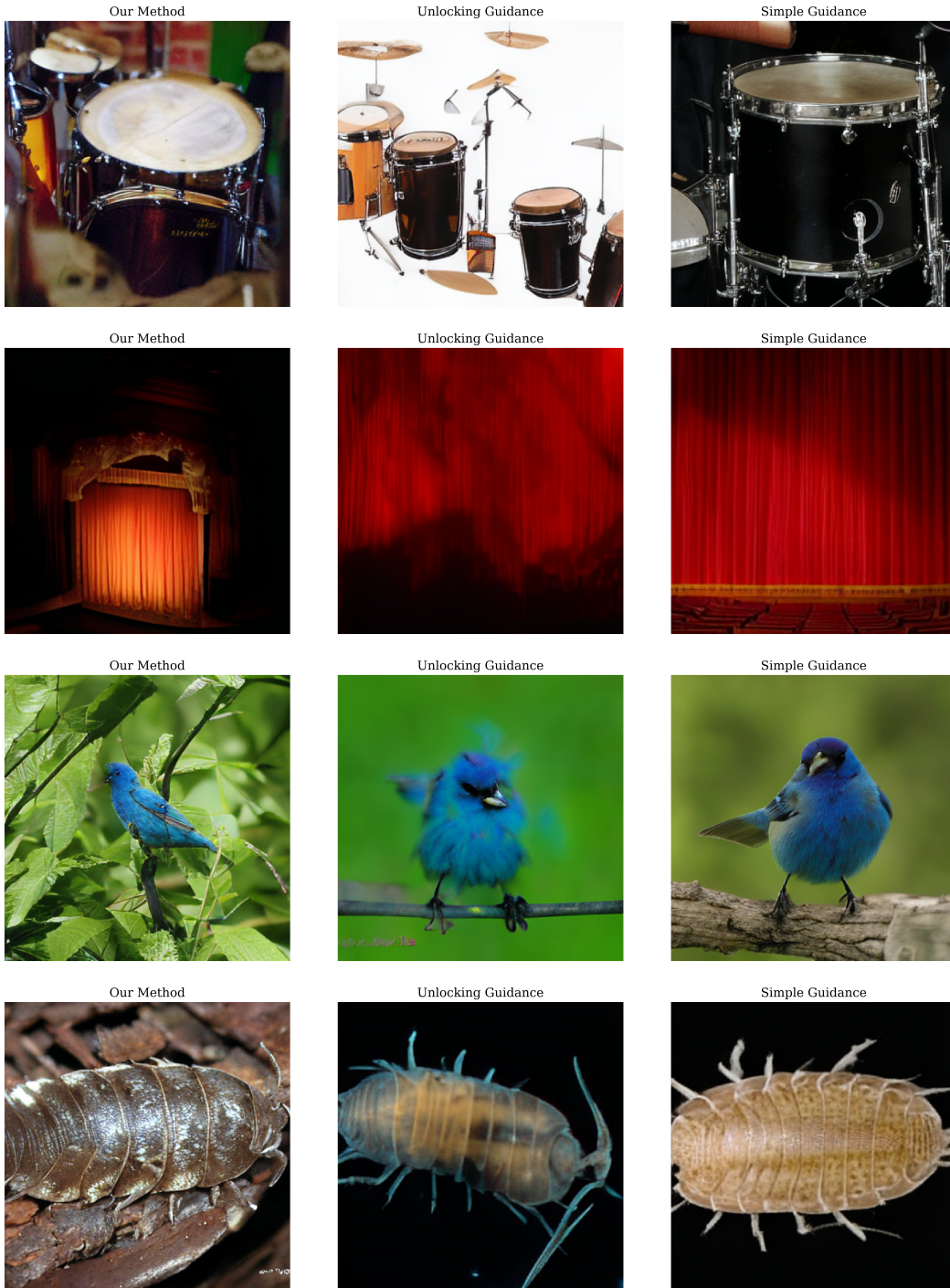


Figure 11: Comparison of samples generated by different guidance methods across various seeds or configurations.

E.4 Guidance strength $w = 5$



Figure 12: Comparison of samples generated by different guidance methods across various seeds or configurations.